CMS Physics Analysis Summary

Contact: cms-pag-conveners-heavyions@cern.ch 2015/06/30

Jet Fragmentation Function in pPb Collisions at $\sqrt{s_{NN}} = 5.02$ TeV and pp Collisions at $\sqrt{s} = 2.76$ and 7 TeV

The CMS Collaboration

Abstract

The fragmentation function of inclusive jets in the pPb collision at $\sqrt{s_{NN}} = 5.02$ TeV is studied, with a dataset corresponding to an integrated luminosity of 31 nb^{-1}. In order to study possible nuclear effects in jet production, this is compared to an pp reference constructed based on the $\sqrt{s} = 2.76$ TeV and $\sqrt{s} = 7$ TeV data, where the fragmentation function is adjusted to the expected flavor mixture at $\sqrt{s} = 5.02$ TeV. The measured pPb fragmentation is found to be consistent with the pp, within the current statistical and systematic uncertainty. This analysis also represents the first CMS measurement of jet fragmentation function at $\sqrt{s} = 7$ TeV, and updates the $\sqrt{s} = 2.76$ TeV jet fragmentation function using pp track and jet reconstruction.

1 Introduction

This analysis is motivated by the recent measurements of the charged particle and jet spectra at high p_{T} in pPb collisions at 5.02 TeV [1, 2]. To reveal the initial and final state modifications of the spectra in heavy ion collisions, one experimental technique is to calculate the ratio of the charged particle p_{T} distribution, or spectra, in heavy ion and pp collisions, scaled by the number of binary nucleon-nucleon collisions [3]. In case of the CMS measurement [1], this nuclear modification factor of charged particles at mid-rapidity, using a reference spectrum interpolated from previous pp measurements at lower and higher collision energies, rises significantly above unity at high p_{T} reaching a value of 1.3–1.4 at $p_{\mathrm{T}} > 40$ GeV/c. The observed enhancement is larger than expected from NLO pQCD predictions [4]. On the other hand, the observed jet nuclear modification factors measured by the CMS and ATLAS collaborations at mid-rapidity only show moderate enhancement (≈ 1.1) [5, 6]. These jet nuclear modification factors are consistent with NLO calculations based on nuclear parton distribution functions (nPDFs). To gain more insights about this intriguing observation, one natural extension beyond the spectra analysis is the measurement of jet fragmentation functions. Naively, given the relative small modification of jet nuclear modification factors and larger enhancement of the high p_{T} charged particle, one would expect that the jet fragmentation functions should be modified in the proton-lead collisions.

In this analysis summary, measurements of jet fragmentation functions in pPb collisions at 5.02 TeV are reported. Jets are reconstructed with an anti-k_t algorithm [7] with distance parameter $R = 0.3$ using particle-flow (PF) event reconstruction [8, 9]. The corresponding pp reference at 5.02 TeV is constructed by an interpolation of 2.76 and 7 TeV pp data. This analysis represents the first CMS measurement of jet fragmentation function at $\sqrt{s} = 7$ TeV. The $\sqrt{s} = 2.76$ TeV jet fragmentation function is also updated, in order to use the pp jet and track reconstruction for the first time.

2 Triggering and Event Selections

This analysis uses the 2.76 TeV pp and 5.02 TeV pPb data taken in 2013, and the high luminosity 7 TeV pp data from 2011.

The High Level Triggers used were chosen to produce a large sample of jets in the jet p_{T} range that they are fully efficient. In the 2.76 TeV pp and 5.02 TeV pPb samples, calorimetric jet triggers with a nominal threshold of 40 and 80 GeV for $R = 0.5$ iterative cone jets were selected for this purpose, with jets having reconstructed p_{T} of 60–100 GeV/c coming from the Jet 40 trigger, and having p_{T} of 100–200 GeV/c coming from the Jet 80 trigger. In the 7 TeV pp samples, triggers with a nominal threshold of 30, 60, and 110 GeV were used to select jets in the p_{T} ranges of 60–80, 80–140, and 140–200 GeV/c, respectively. Events are also required to have the z position of the vertex with the highest p_{T}^2 sum from associated tracks to be within 15 cm of the center of the detector.

3 Charged Particle Reconstruction

Charged particles are reconstructed using the same iterative method [10] as in previous CMS analyses of pp collisions. This is done even in pPb systems, as the detector occupancy is still low enough for the pp reconstruction to perform well. Tight track quality selection criteria are applied to reduce the rate of background rate for falsely reconstructed ("fake") tracks and secondary interactions ("secondary" particles, originating from conversion, nuclear interaction

with detector material, and decay of long-lived particles such as K^0_L and Λs), as tracks are required to satisfy the "high purity" selection [10].

The track reconstruction efficiency and fake rate depend on the η, ϕ, p_{T} of the track, and on the local charged particle density. The local charge particle density is directly affected by the presence of jets in the event. Therefore, the corrections for efficiency and fake rate are evaluated as a function of η, ϕ, $p_{\mathrm{T}}^{\mathrm{track}}$, and $p_{\mathrm{T}}^{\mathrm{jet}}$ (the p_{T} of the closest jet with $p_T^{\mathrm{jet}} > 60\,\mathrm{GeV}/c$ to the track) using PYTHIA+HIJING simulation [11–13].

In pp and pPb collisions, the track reconstruction efficiency is $\sim$ 90% at 10 GeV/c and 80% at 0.5 GeV/c for tracks selected for analysis. The fake tracks is $< 2\%$ for $p_{\mathrm{T}} > 1\,\mathrm{GeV}/c$ and slightly higher below this value. The contribution of particles from secondary particles are subtracted as the secondary particle rate goes as high as 2%. The rate of reconstructing a single charged particles into multiple tracks is smaller than 1% and it is not corrected for. A simple secondary particle correction is applied as it is evaluated only according to the η and p_{T} values of charged particles.

4 Jet Reconstruction

Jet reconstruction in this analysis is performed with the anti-k_t jet algorithm that is encoded in the FastJet framework [14]. The jet reconstruction algorithm used in this analysis is chosen to be identical to the dijet asymmetry analysis in pPb collisions [15]. A distance parameter of $R = 0.3$ is used to minimize the effects of heavy ion underlying event fluctuations. This choice of jet algorithm and cone size allows a direct comparison between the pPb results and previously published PbPb data.

For the 2.76 TeV pp and 5.02 TeV pPb data, since there is negligible amount of pileup, the anti-k_t algorithm is used on the reconstructed PF objects. In the 7 TeV pp data collected in 2011, on the other hand, there is significant amount of pile up. The standard high luminosity pp reconstruction employed by CMS for this data set is followed, where the jet energy is first corrected by clustering the entire event, observing the median p_T density ρ from all jets, and subtracting the so determined pileup offset $(-\rho A)$, where A is the area occupied by each reconstructed jet. After correcting for the jet energy scale in PYTHIA tune Z2 Monte Carlo (MC) (The PYTHIA 6 tune Z2 is identical to tune Z1 [16] with the exception of CTEQ5L parton distribution function (PDF) being updated to CTEQ6L1), the dijet balance and γ+jet balance are used to further correct the residual data-to-MC difference in all three systems, as detailed in [15].

5 Analysis

The construction of the fragmentation functions begins by selecting jets out of the fully efficient region of a trigger path's turn on. The path is selected depending on the measured jet p_{T} range, as detailed in Section 2. The jets are required to have a raw p_{T} of more than 30 GeV/c, and the contribution of charged particles to the total raw p_{T} must be between 5 and 95%. This cut helps reject fake 'neutral' jets that have no charged particles and are a result of calorimeter noise, as well as jets with just a single high p_{T} charged particle. Jets are also required to have $|\eta_{CM}| < 1.5$, where η_{CM} is the pseudorapidity in the center of mass frame of the colliding system. For the two pp systems this frame corresponds to the lab frame, but for the pPb system this frame differs from the lab frame by a rapidity boost of 0.45. After selection and jet quality cuts, the jets are binned into five bins according to their reconstructed p_{T}.

For all of the jets in each bin, the tracks within a distance parameter of $R = 0.3$ of the jet are

tabulated as a function of their p_{T}. This distance parameter was chosen because it coincides with the distance parameter of the jet reconstruction algorithm, although it is possible that tracks within $R = 0.3$ are not in the reconstructed jet due to way the jet reconstruction algorithm clusters tracks together. These tracks are required to pass a quality selection and are corrected for losses due to detector acceptance and efficiency, as detailed in section 3. Tracks having a p_{T} greater than the maximum jet p_{T} allowed in each jet p_{T} bin are not selected.

In the 5.02 TeV pPb collision system, and also the 7 TeV pp system with pile-up, the event contains energy not originating from the hard scattering. In order to subtract tracks from these sources, for every jet used in the analysis another set of tracks in some other cone of the distance parameter of $R = 0.3$ are also tabulated and corrected. The location and system that this second cone is in depends on the type of underlying event subtraction being performed. In this analysis, two different underlying event methods are used. The first method uses a second cone that is rotated 90 degrees in ϕ from the original jet cone. This method has the advantage of sampling the same underlying event as the first cone, but could also possibly pick up very widely radiated particles originating from the original jet. This is the method used when reporting the underlying event subtracted results in this analysis. The second method attempts to match a minimum bias event ("second event") having similar underlying event activity to first event, containing the jet, for which the fragmentation function is calculated with ("first event"). The second cone is then located in the same location as the first cone, but tracks in the second event are used to tabulate the background. This method is used as a cross check of the first method, and allows us to estimate the systematic uncertainties associated with the underlying event subtraction. After counting the unnormalized underlying event track spectrum in this second cone, it is then subtracted from the previously calculated track spectrum. The resulting spectrum is then divided by the bin width to make it differential, and also normalized by the inverse of the number of jets in the jet p_{T} bin used to yield the fragmentation function.

A similar procedure is done when calculating the fragmentation functions as a function of ξ, which is defined as the log of ratio of the jet momentum with the component of the track's momentum parallel to the jet:

$$\xi = \log \frac{p^{jet}}{p_{||}^{track}} \tag{1}$$

In this case, instead of tabulating the p_{T} spectrum of each jet, the ξ spectrum is used instead. For the purposes of underlying event subtraction, the underlying event tracks are treated as being in the cone of a jet having the same magnitude of momentum as the matching original jet.

6 Interpolated pp Reference

In order to compare the pPb jet fragmentation function to the fragmentation function in pp, a 5.02 TeV pp reference must be constructed. This analysis uses a data-driven approach, by interpolating known data taken at 2.76 and 7 TeV. The validity of this interpolation procedure is based on the assumption that the fragmentation function of a quark jet having a specific p_{T} will be the same as another quark jet having the same p_{T}, regardless of the $\sqrt{s}$ of the collision that produced the jet. It is assumed that the previous statement is also true for gluon jets. The total fragmentation function of a jet at a given p_{T} will then be some linear combination of these two quark and gluon fragmentation functions, with the coefficients of the linear combination simply being the quark fraction and gluon fraction of the jets produced. It should be noted that these quark and gluon fractions do, in fact, change with the collisions $\sqrt{s}$; therefore we

use PYTHIA to model these fractions, which can be seen in Fig. 1 for both reconstructed and generator level jet p_{T}.

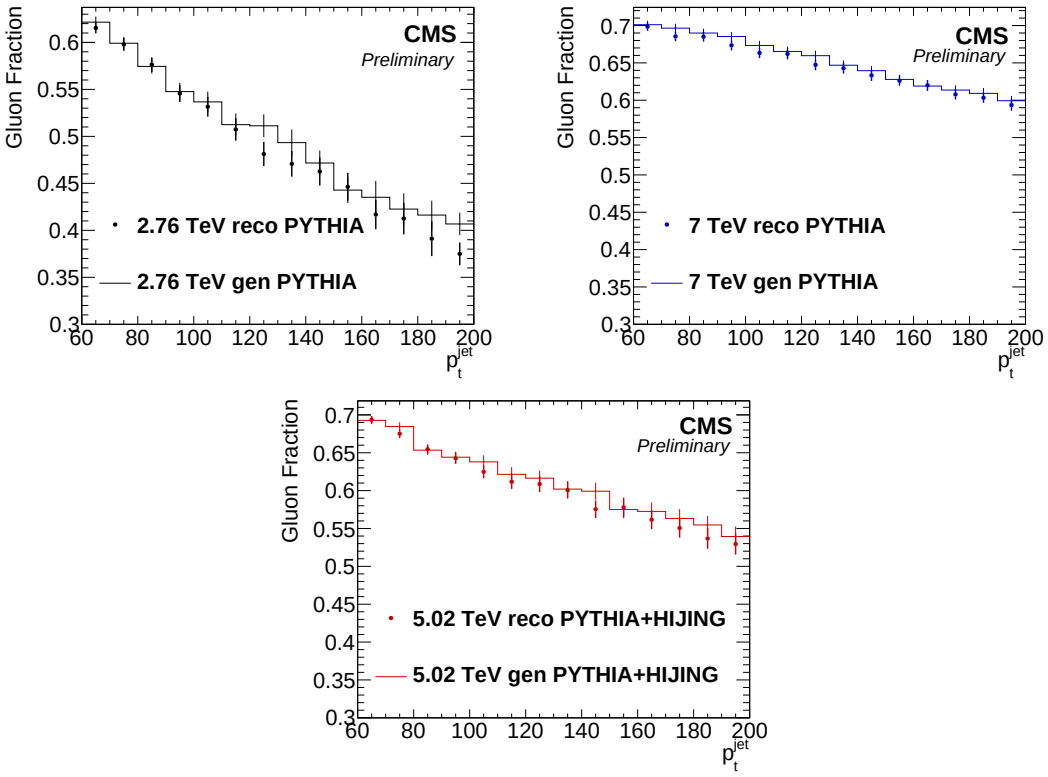

Figure 1: The gluon fraction of jets in PYTHIA (or PYTHIA+HIJING) at the three different center of mass energies studied here. The horizontal axis correspondes to reconstructed jet p_{T} for reco information, and generator level jet p_{T} for gen information.

First the fragmentation functions of the 2.76 and 7 TeV pp data are calculated in the desired jet p_{T} bins. While doing this, the jet p_{T} spectra is reweighted to equal that of the 5.02 TeV pPb data in order to prevent the larger amount of jets produced at 7 TeV from biasing the interpolation towards the 7 TeV data, and to allow direct comparison of the interpolated function to the 5.02 TeV pPb data. Let F_2 and F_7 be the 2.76 and 7 TeV pp fragmentation functions after jet spectrum reweighting. Call the quark and gluon fragmentation functions at 5.02 TeV Q and G, respectively. Note that these quantities are functions of the reconstructed track p_{T}. Finally, the gluon fraction of jets at 2.76 and 7 TeV is represented by r_2 and r_7, whereas the quark fractions are simply given by $1 - r$. These two fragmentation functions can then be rewriten in terms of the quark and gluon fragmentation function basis as follows

$$F_2 = r_2 G + (1 - r_2) Q \tag{2}$$
$$F_7 = r_7 G + (1 - r_7) Q \tag{3}$$

This can be solved for Q and G:

$$G = \frac{(1-r_7)F_2 - (1-r_2)F_7}{r_2 - r_7} \quad (4)$$

$$Q = \frac{-r_7 F_2 + r_2 F_7}{r_2 - r_7} \quad (5)$$

Now since r_5 is known from Monte Carlo, we can immediately construct the interpolated pp reference at 5.02 TeV, F_5:

$$F_5 = r_5 G + (1-r_5)Q = \frac{(r_5 - r_7)F_2 + (r_2 - r_5)F_7}{r_2 - r_7} \quad (6)$$

7 Results

The fragmentation functions of jets in the range of 60 to 200 GeV/c have been measured for 2.76 and 7 TeV pp collisions, and are shown in Fig. 2 before any jet p_{T} spectrum reweighting is done for the interpolation construction. Additionally, the fragmentation functions were measured in 5.02 TeV pPb collisions, and a 5.02 TeV pp reference has been constructed using an interpolation of the 2.76 and 7 TeV data, shown in Fig. 3. The ratio of the pPb fragmentation with respect to this pp reference is consistent with unity at high track p_{T}, as shown in Fig. 4. The results after a ϕ rotated background subtraction method has been applied are shown in Fig. 5–7. The application of the background subtraction largely removes the excess in the low-p_{T} of the fragmentation function, showing that it is primarily caused by the pPb underlying event.

The same results have been plotted as a function of the variable ξ in Figs. 8 through 13.

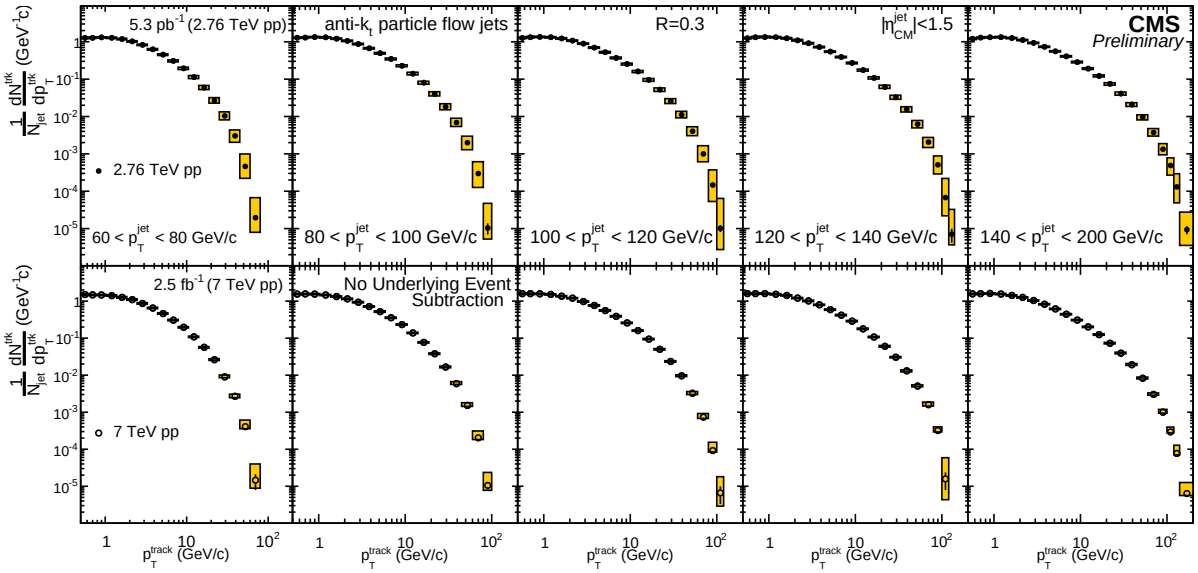

Figure 2: The measured fragmentation functions in pp systems for $R = 0.3$ anti-k_t jets with $|\eta| < 1.5$, without any underlying event subtraction. The fragmentation functions (top row) for 2.76 TeV, and (bottom row) for 7 TeV. Starting from the leftmost column, fragmentation functions for jets with increasing p_T are shown.

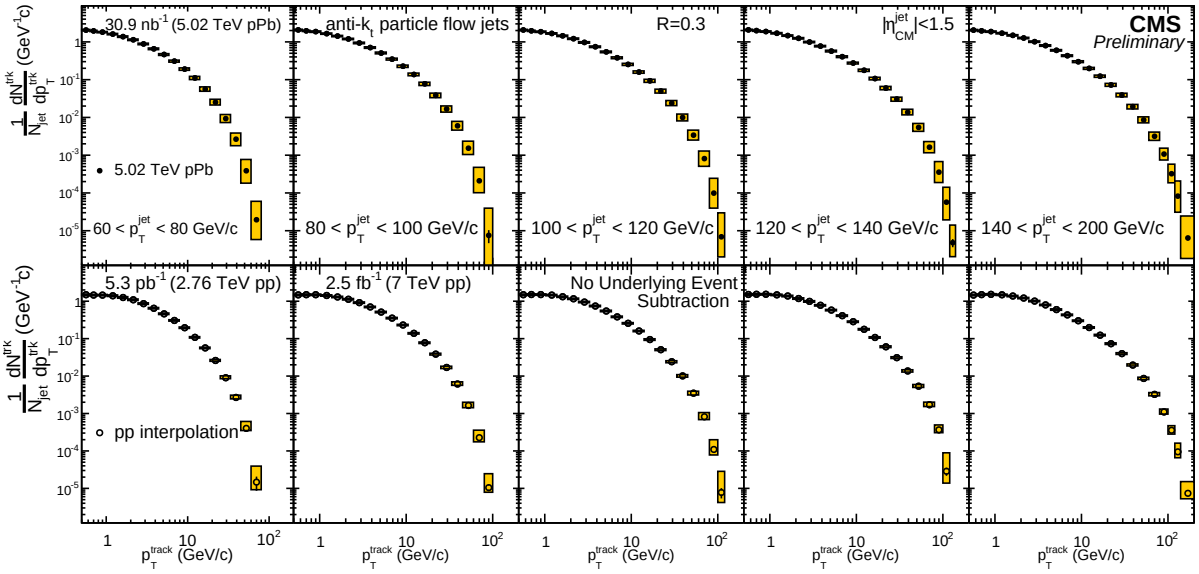

Figure 3: (Top row) the measured fragmentation functions in 5.02 TeV pPb for $R = 0.3$ anti-k_t jets with $|\eta_{\mathrm{CM}}| < 1.5$. (Bottom row) the interpolated pp reference constructed from 2.76 and 7 TeV pp measured fragmentation functions and the same kinematic selection. No underlying event subtraction is performed, so there is an excess at low track p_{T}.

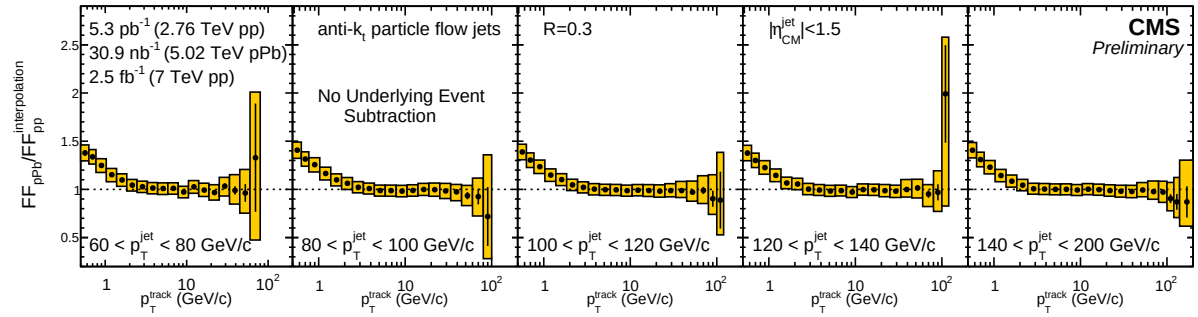

Figure 4: Ratio of the pPb and pp reference. Starting from the leftmost column, fragmentation functions for jets with increasing p_T are shown. No underlying event subtraction is performed, so there is an excess at low track p_{T}.

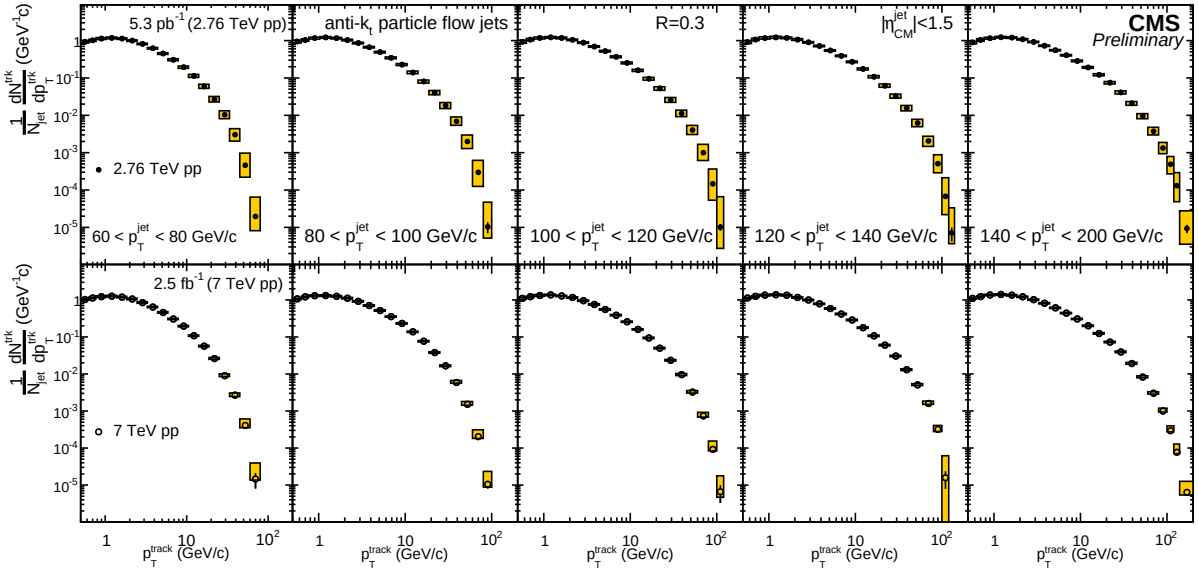

Figure 5: The measured fragmentation functions in pp systems for $R = 0.3$ anti-k_t jets with $|\eta| < 1.5$, with underlying event subtraction done using a 90 degree rotated cone in the ϕ direction. The fragmentation functions (top row) for 2.76 TeV, and (bottom row) for 7 TeV. Starting from the leftmost column, fragmentation functions for jets with increasing p_T are shown.

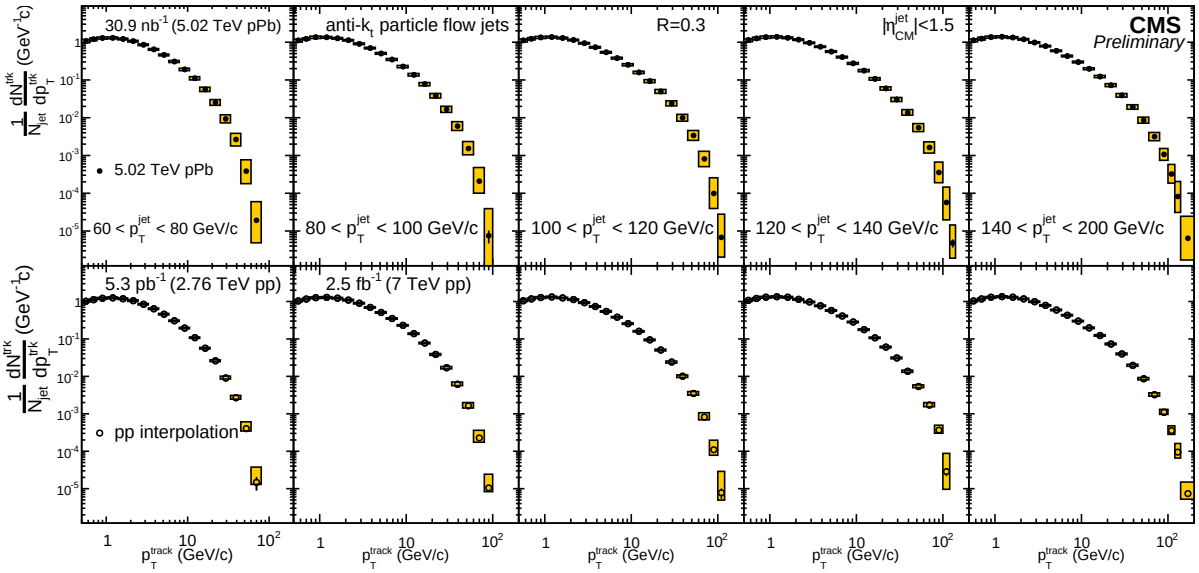

Figure 6: (Top row) The measured fragmentation functions in 5.02 TeV pPb for $R = 0.3$ anti-k_t jets with $|\eta_{\mathrm{CM}}| < 1.5$. (Bottom row) The interpolated pp reference constructed from 2.76 and 7 TeV pp measured fragmentation functions and the same kinematic selection. Underlying event subtraction has been done using a 90 degree rotated cone in the ϕ direction.

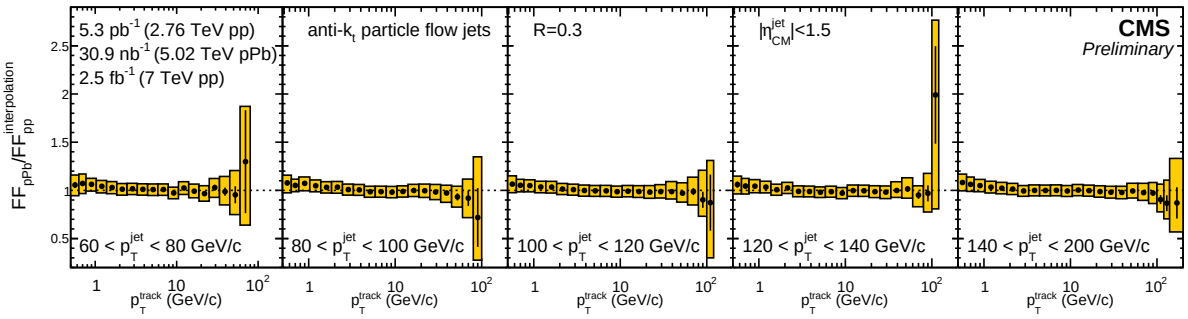

Figure 7: Ratio of the pPb and pp reference. Starting from the leftmost column, fragmentation functions for jets with increasing p_T are shown. Underlying event subtraction has been done using a 90 degree rotated cone in the ϕ direction.

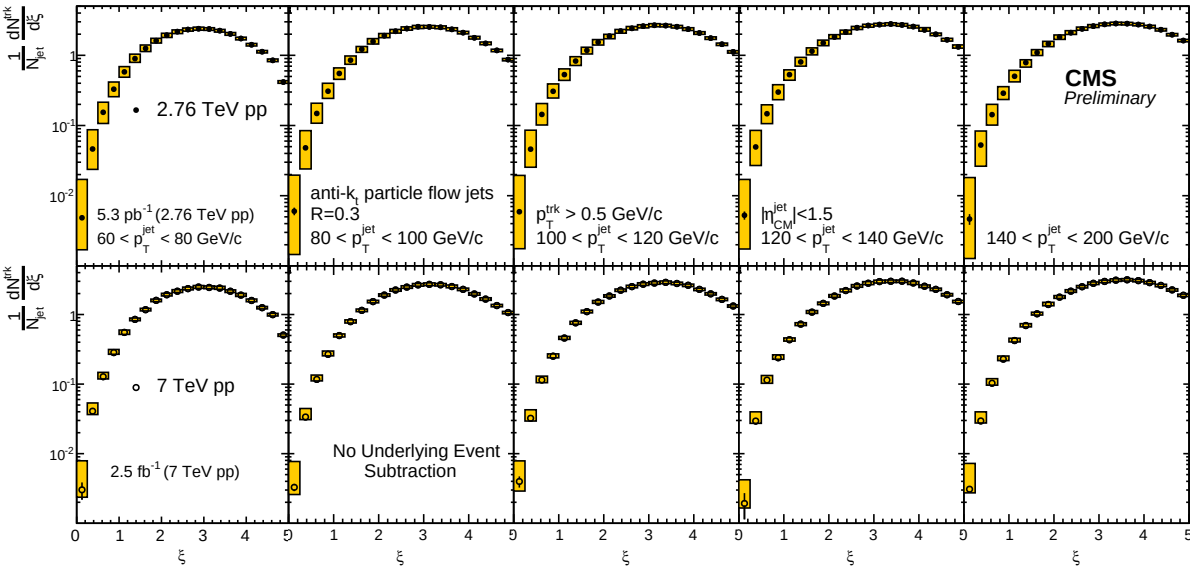

Figure 8: The measured fragmentation functions in pp systems for $R = 0.3$ anti-k_t jets with $|\eta| < 1.5$, without any underlying event subtraction as a function of ξ. The fragmentation functions (top row) for 2.76 TeV, and (bottom row) for 7 TeV. Starting from the leftmost column, fragmentation functions for jets with increasing p_T are shown.

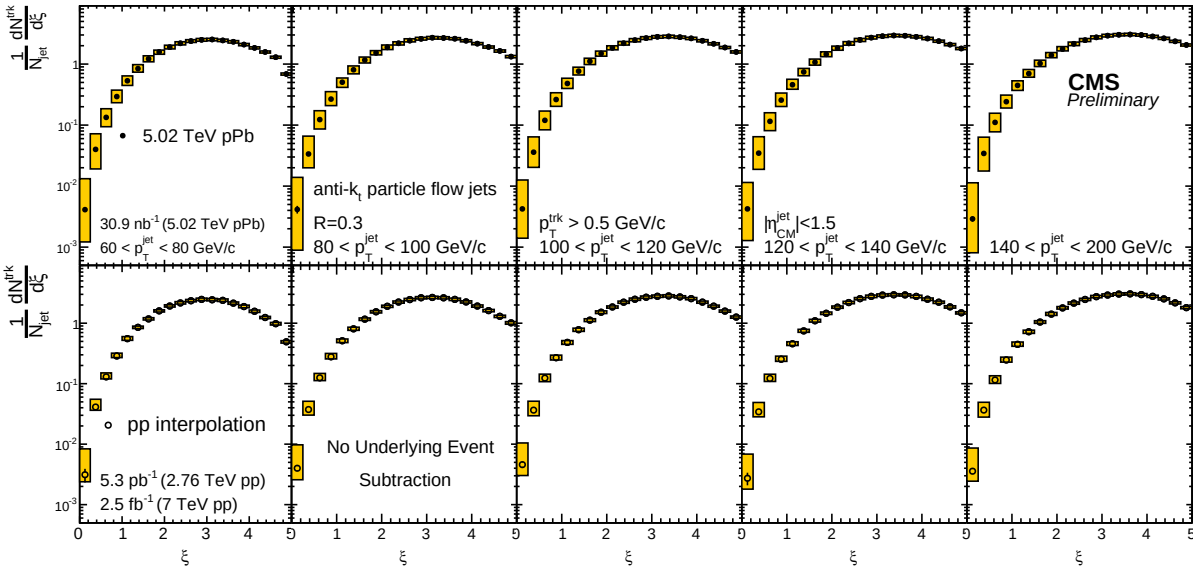

Figure 9: (Top row) The measured fragmentation functions in 5.02 TeV pPb, plotted as a function of ξ for $R = 0.3$ anti-k_t jets with $|\eta_{\mathrm{CM}}| < 1.5$. (Bottom row) The interpolated pp reference constructed from 2.76 and 7 TeV pp measured fragmentation functions and the same kinematic selection. No underlying event subtraction is performed, so there is an excess at low track p_{T}.

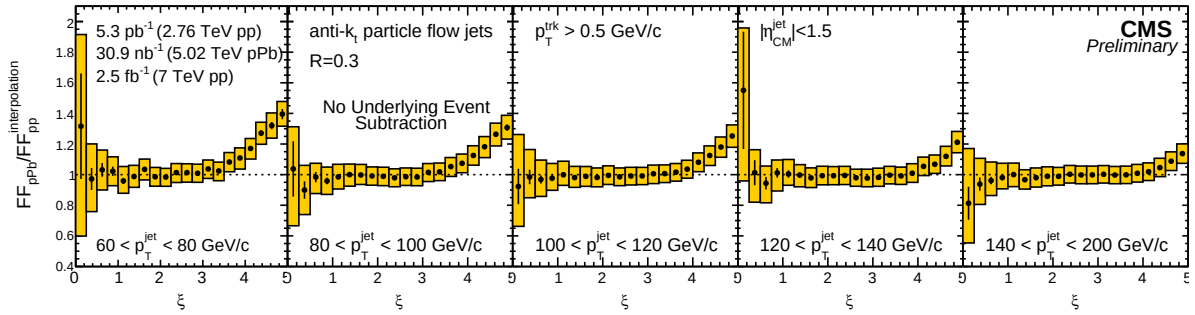

Figure 10: Ratio of the pPb and pp reference. Starting from the leftmost column, fragmentation functions for jets with increasing p_T are shown. No underlying event subtraction is performed, so there is an excess at low track p_{T}.

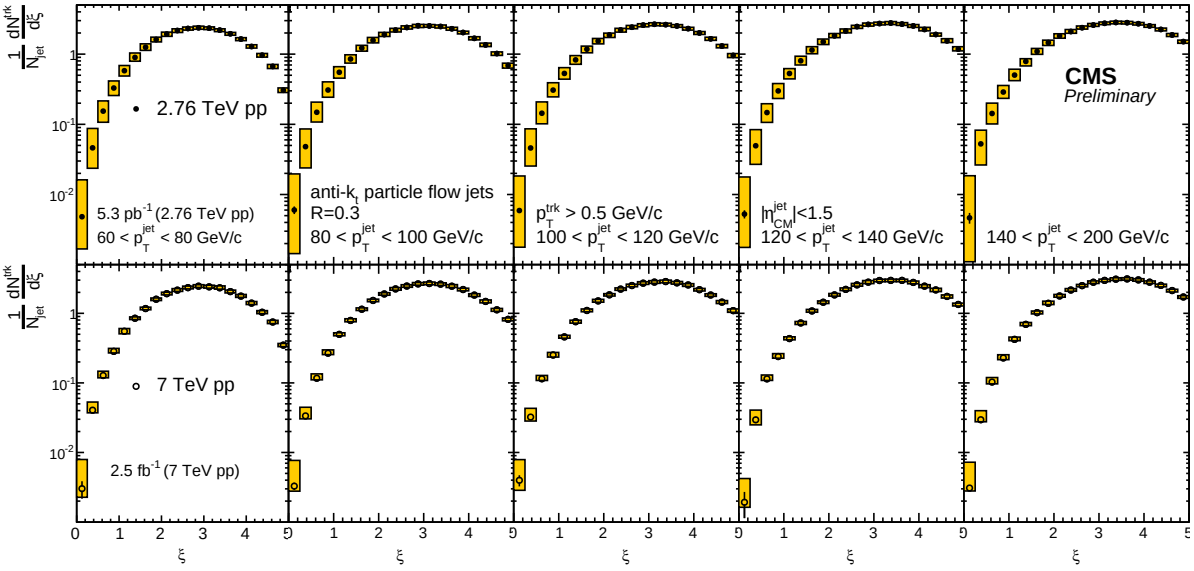

Figure 11: The measured fragmentation functions in pp systems for $R = 0.3$ anti-k_t jets with $|\eta| < 1.5$, with underlying event subtraction using a 90 degree rotated cone in the ϕ direction, plotted as a function of ξ. The fragmentation functions (top row) for 2.76 TeV, and (bottom row) for 7 TeV. Starting from the leftmost column, fragmentation functions for jets with increasing p_T are shown.

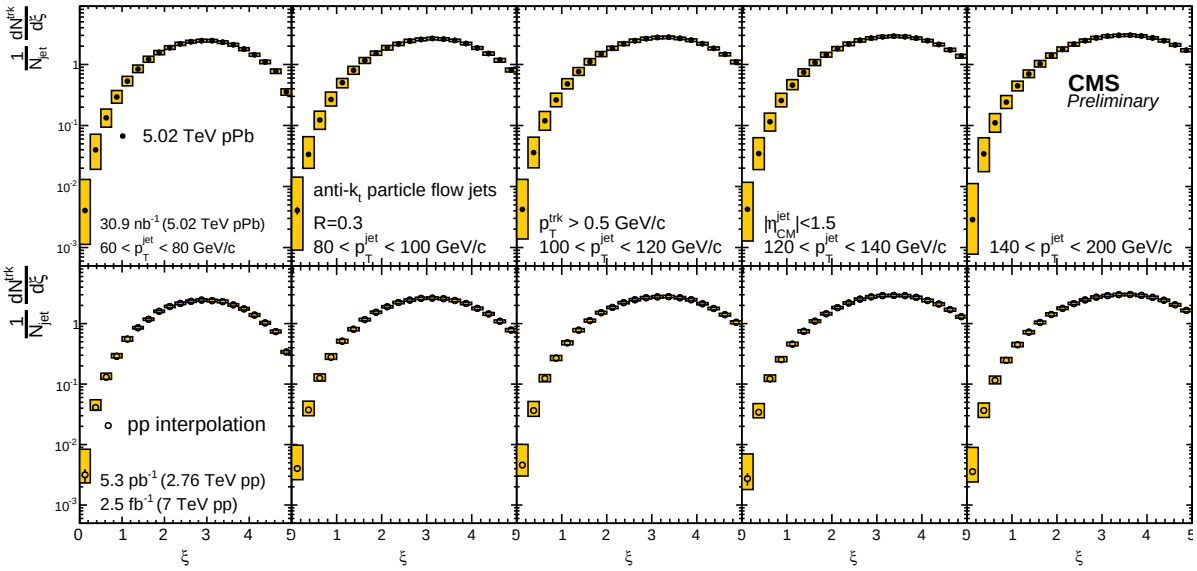

Figure 12: (Top row) The measured fragmentation functions in 5.02 TeV pPb for $R = 0.3$ anti-k_t jets with $|\eta| < 1.5$, plotted as a function of ξ. (Bottom row) The interpolated pp reference constructed from 2.76 and 7 TeV pp measured fragmentation functions and the same kinematic selection. Underlying event subtraction has been done using a 90 degree rotated cone in the ϕ direction.

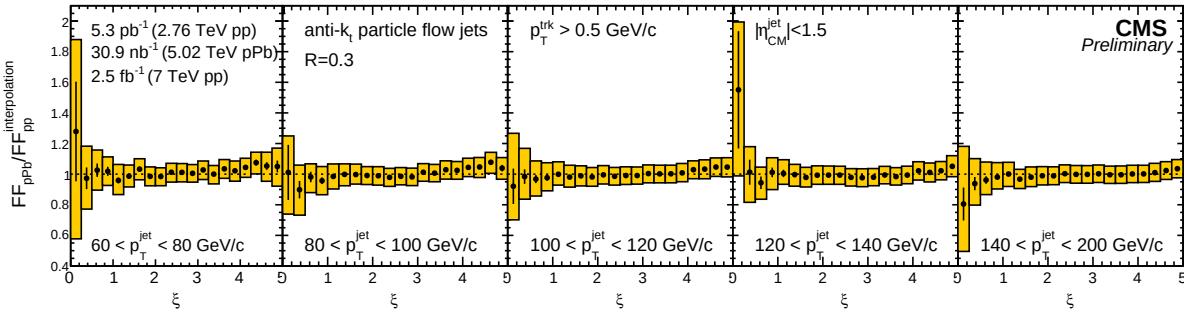

Figure 13: Ratio of the pPb and pp reference. Starting from the leftmost column, fragmentation functions for jets with increasing p_T are shown. Underlying event subtraction has been done using a 90 degree rotated cone in the ϕ direction.

8 Systematics

A flat 3.9% systematic uncertainty is quoted for tracking performance differences between data and Monte Carlo samples in each fragmentation function. Any remaining systematic uncertainty due to nonclosure of tracking corrections in Monte Carlo is contained in the reconstructed-to-generator truth difference described later in this section. Due to cancellation, taking a ratio of two fragmentation functions significantly reduces the tracking correction-related systematic uncertainty.

Changes in the jet energy scale (JES) affect the fragmentation function result because it can shift jets with a higher p_{T} into a fragmentation function bin, making the fragmentation harder if the JES is underestimated. On the other hand, if the JES is overestimated, low p_{T} jets will be shifted into the bin and make the fragmentation softer. In order to evaluate this effect on the result, the JES was varied up and down by the uncertainty of the jet momentum for each of the three systems: 2.76 TeV pp, 5.02 TeV pPb, and 7 TeV pp. The uncertainty of the jet momentum was taken from 7 and 8 TeV global analyses, which yields η and p_{T} dependent values [17]. For the jet energy correction, separate correction factors were used for the individual collision systems, as the detector response have changed between the 2011 and 2013. The ratio of the modified result was taken with the unmodified result, and the observed deviation from unity is taken as a sytematic uncertainty. The uncertainties are evaluated asymmetrically here, and the effects of modifying the JES of different systems were added in quadrature under the conservative assumption that the JES are uncorrelated. The high track p_{T} part of each fragmentation function is very sensitive to variations in the JES, making this one of the dominant systematics at high track p_{T}. If the uncertainty in a given bin is less than 0.1%, a value of 0.1% is used instead.

The Jet Energy Resolution (JER) is estimated to be 10% of the jet p_{T} in all three systems used in this analysis. In order to see how the results of the analysis varied due to fluctuations in the JER, the jet p_{T} was smeared by an additional 5%, amounting to a 1% increase in the total JER from 10% to 11%. The ratio of this modified result was taken with the unmodified result, and this was taken as the systematic uncertainty owing to the JER.

The interpolation procedure used to construct the pp reference in this analysis relies on the assumption of QCD factorization at leading order. Thus, it is possible that small nonclosure exists due to higher order effects. Furthermore, the gluon fractions used in the analysis are taken from MC samples and therefore do not necessarily represent the exact gluon fractions in data. This is due to uncertainties in the PDF used to generate the flavor of the hard scattering processes modeled. In order to take into account these two effects, generator-level MC production, at the three $\sqrt{s}$ used in this analysis, is repeated for different PDF fits. These different samples were used to calculate the difference in the quark-to-gluon ratio. This quark-to-gluon ratio was then used in the interpolation procedure to see the effect each different PDF fit has on the interpolated spectrum. A fit to the variation in the p_{T}-dependent, interpolated quark-to-gluon ratio for the NNPDF 2.1 LO [18] was then performed to extract the uncertainty of the PDF variation. As a result of these studies, a systematic uncertainty of 0.5% has been assigned to the pp interpolation to take into account both generator-level nonclosure of the interpolation procedure and the uncertainties associated with the PDF used by the MC generator.

The same procedure done in the analysis was applied to Monte Carlo samples. At generator level, the interpolation of the 2.76 TeV and 7 TeV PYTHIA samples matches the fragmentation of the 5.02 TeV PYTHIA+HIJING sample in the regime of track p_{T} where the underlying event is negligible. This indicates that the interpolation procedure does adequately reproduce the 5.02 TeV jet fragmentation at generator level. The leftover difference between reconstructed and generator level Monte Carlo is quoted bin by bin as a systematic uncertainty in all measure-

ments shown.

In this analysis a cut requiring the fraction of each jet's raw p_{T} coming from charged charged particles to be between 5 and 95% is applied. Although this cut helps reject fake jets, it could also possibly bias the fragmentation function measurement. In order to account for this potential bias in the systematic uncertainty, the full analysis procedure was redone without the charge fraction cut in data. The difference between the result with and without the jet charge fraction cut was then taken as a systematic uncertainty.

Halfway through the collection of the pPb data set used in this analysis, the directions of the proton and lead beams circulating in the LHC was reversed. This effectively leads to different detector conditions between the two sets of data. In order to evaluate the effect of this beam reversal on the analysis, the data set was split into its pPb-going and Pbp-going parts and repeated on each half. The ratio of the Pbp and pPb fragmentation functions is consistent with one for the highest jet p_{T} bins, but shows a small difference in some bins at lower jet p_{T}. In order to account for this, half the difference between the pPb and Pbp results is taken as a systematic in our analysis.

The underlying event subtraction using a 90 degree rotated cone in the ϕ direction is checked by using a minimum bias event mixing subtraction method, as described earlier in this summary. The ratio of the two methods is calculated and taken as a systematic uncertainty. This uncertainty is up to 10% at very low track p_{T}, but rapidly shrinks to 0 at a p_{T} of around 5 GeV/c.

Summaries of the various contributions to the systematic uncertainties are shown for chosen bins for the pPb fragmentation function in Table 1, and for the fragmentation function ratio in Table 2.

The jet energy scale and resolution are the dominant source for the fragmentation function at high p_T or small ξ. The systematic uncertainties are significantly smaller in pp collisions used to construct the fragmentation function reference, this also causes the pp interpolation to have smaller systematic uncertainties than pPb data. For our kinematic selection, the pp jet energy scale uncertainty ranges from 0.7%–1.6%, the pPb jet energy scale uncertainty ranges from 0.8%–2.3%.

Table 1: Summary of the systematic uncertainies in the 5.02 TeV pPb fragmentation function with a 90-degree ϕ rotated underlying event (UE) subtraction as a function of track p_{T}. The p_{T} values are given in units of GeV/c.

	$60 < p_T^{jet} < 80$			$140 < p_T^{jet} < 200$		
	$0.5 < p_T^{track} < 5.9$	$5.9 < p_T^{track} < 45$	$45 < p_T^{track} < 200$	$0.5 < p_T^{track} < 5.9$	$5.9 < p_T^{track} < 45$	$45 < p_T^{track} < 200$
Symmetric uncertainty source						
Tracking	3.9%	3.9%	3.9%	3.9%	3.9%	3.9%
PDF + gen interpolation	0.5%	0.5%	0.5%	0.5%	0.5%	0.5%
JER	0.1 – 1.9%	0.1 – 2.1%	0.1 – 3%	0 – 0.7%	0.1 – 0.9%	0.5 – 19%
pPb/Pbp difference	0 – 0.5%	0.1 – 1.7%	4.6 – 14%	0.1 – 2%	0.1 – 1%	0.1 – 3.9%
UE subtraction	0.8 – 8.9%	0.1 – 0.3%	0.5 – 1.5%	1 – 7.8%	0.1 – 0.4%	0 – 0.4%
Asymmetric uncertainty source						
JES (upwards uncert.)	0.4 – 3.3%	5.2 – 26%	88 – 170%	0.1 – 1.6%	2 – 11%	19 – 250%
JES (downwards uncert.)	-0.6 – -2.8%	-4.4 – -21%	-53 – -73%	-0.1 – -1.4%	-2.4 – -9.3%	-16 – -71%
Reco/gen difference	-1.8 – 1.4%	0.4 – 6.8%	31 – 82%	-0.7 – 3.4%	1.7 – 4.1%	1.1 – 78%
Jet charge fraction cut	-1 – 0.3%	-0.4 – 6.6%	36 – 92%	-1.5 – -0.8%	-1 – 1.5%	5.6 – 110%
Total (upwards uncert.)	4.8 – 10%	6.5 – 28%	100 – 210%	4.6 – 9.1%	5.3 – 12%	21 – 280%
Total (downwards uncert.)	-4.9 – -10%	-5.9 – -22%	-53 – -75%	-4.5 – -8.9%	-4.8 – -10%	-17 – -73%

Table 2: Summary of the systematic uncertainies in the fragmentation function ratio with a 90-degree ϕ rotated underlying event (UE) subtraction as a function of track p_{T}. p_{T}s are given in units of GeV/c.

	$60 < p_T^{jet} < 80$			$140 < p_T^{jet} < 200$		
	$0.5 < p_T^{track} < 5.9$	$5.9 < p_T^{track} < 45$	$45 < p_T^{track} < 200$	$0.5 < p_T^{track} < 5.9$	$5.9 < p_T^{track} < 45$	$45 < p_T^{track} < 200$
Symmetric uncertainty source						
Tracking	5.5%	5.5%	5.5%	5.5%	5.5%	5.5%
PDF + gen interpolation	0.5%	0.5%	0.5%	0.5%	0.5%	0.5%
JER	0.4 – 2%	0.2 – 2.8%	0.4 – 4.4%	0.2 – 0.6%	0.3 – 1.1%	2.4 – 22%
pPb/Pbp difference	0 – 0.6%	0.2 – 1.8%	4.8 – 15%	0.1 – 2%	0.1 – 1%	0.8 – 3.6%
UE subtraction	0.1 – 7.6%	0.1 – 0.4%	0.9 – 2.4%	0.1 – 5.5%	0 – 0.1%	0 – 0.4%
Asymmetric uncertainty source						
JES (upwards uncert.)	0.4 – 2%	1.4 – 6.5%	24 – 36%	0.3 – 1.4%	0.8 – 2.4%	4.7 – 39%
JES (downwards uncert.)	-0.4 – -1.7%	-1.5 – -7.1%	-19 – -35%	-0.4 – -1%	-0.8 – -2.4%	-3.9 – -26%
Reco/gen difference	-4.4 – -1.7%	-1.9 – 0.9%	-33 – -6.2%	-1 – 2%	-0.2 – 1%	-5.3 – 8.4%
Jet charge fraction cut	-0.6 – 2.2%	-0.1 – 0.6%	5.7 – 20%	-0.4 – 0.5%	-0.1 – 0.2%	0.7 – 28%
Total (upwards uncert.)	5.6 – 9.8%	5.7 – 9.2%	26 – 44%	5.6 – 8%	5.7 – 6.3%	8.1 – 53%
Total (downwards uncert.)	-5.9 – -11%	-6 – -9.8%	-22 – -51%	-5.6 – -7.9%	-5.6 – -6.2%	-7.4 – -35%

9 Comparison to pPb Nuclear Modification Factor Analysis

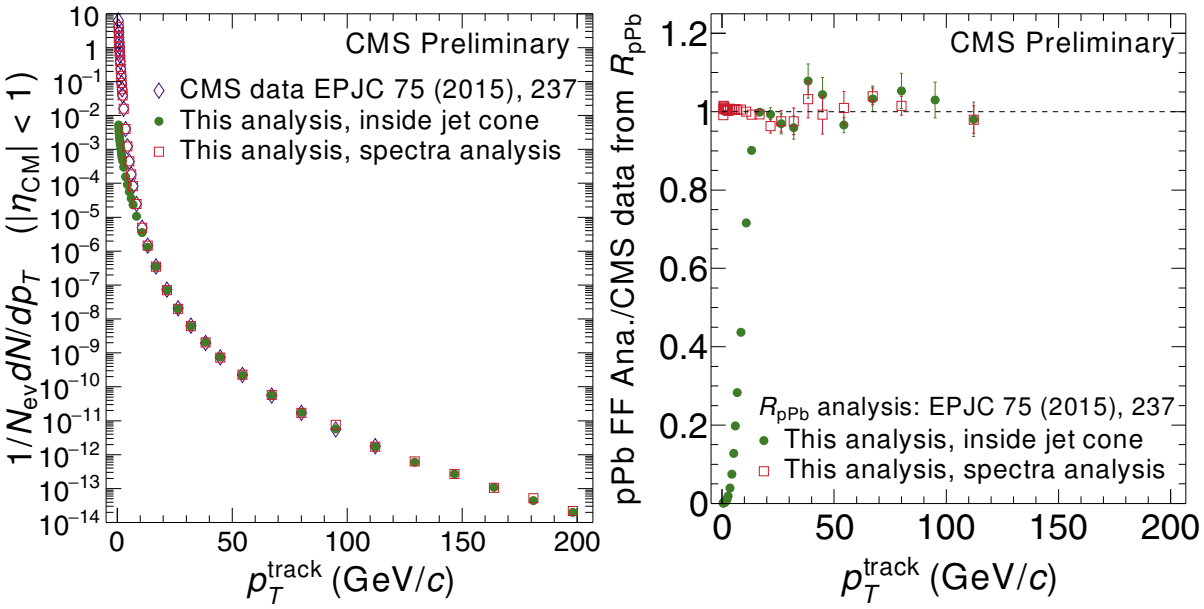

Figure 14: The measured particle spectrum (left) in 5.02 TeV pPb, and the in-cone component, compared to [1]. All tracks > 40 GeV/c originate from jets > 60 GeV/c. Both analyses differ in their triggers and tracking correction. A ratio is also shown (right).

The total set of tracks entering this analysis is compared to the pPb spectrum in [1] for consistency. Both analyses differ in their triggers and tracking correction, but it can be seen from this comparison that for the pPb result entering in both analysis, there is virtually no difference. Also compared is a variation of this analysis, where the tracks is not required to originate within $\Delta R < 0.3$ of the jet, essentially turning this analysis into a spectra measurement. It can be seen that, when tracks > 40 GeV/c originate from jets > 60 GeV/c, all three measurement agree to $< 5\%$. Also, the spectra measurement mode of this analysis agrees with [1] down to the lowest track $p_T = 500$ MeV used in this analysis. Figure 14 shows a comparison of the charged particle spectra, and their ratios.

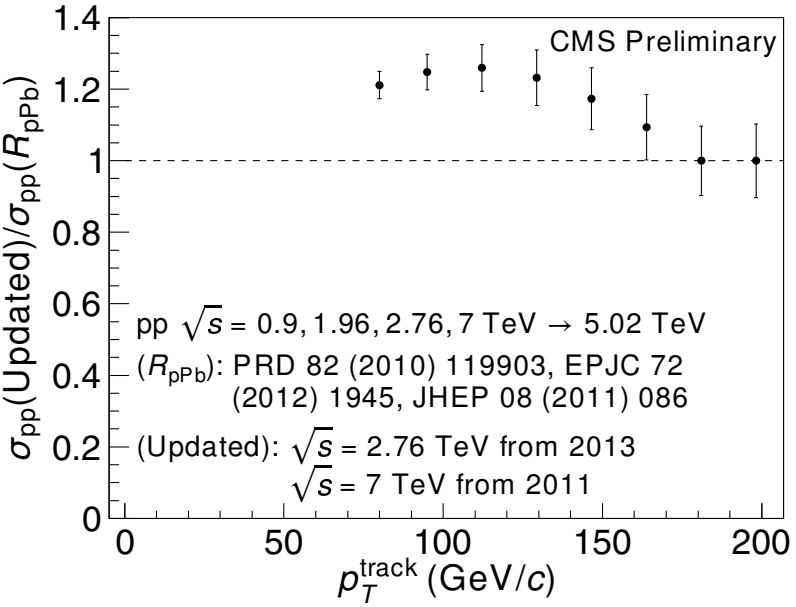

Figure 15: Ratio of the pp reference spectrum at 5.02 TeV, when using the 0.9, 1.96, 2.76, and 7 TeV spectra from [19–21], or when replacing 2.76 and 7 TeV spectra from the aforementioned $\sqrt{s}$ using the spectra from this analysis. In both cases, the x_T-based interpolation in [1] is used.

To investigate the potential difference in the pp reference, two scenarios when constructing the 5.02 TeV pp reference are compared. First the 0.9, 1.96, 2.76, and 7 TeV spectra from [19–21] are interpolated by the x_T-based method in [1]. Then running this analysis as a spectra analysis, the resulting 2.76 TeV and 7 TeV charged particle spectra are combined with the previous 0.9 and 1.96 TeV results, then a x_T-based interpolation to 5.02 TeV is obtained. Figure 15 shows the ratio between the two interpolation results.

10 Summary

The inclusive jet fragmentation function for pPb collisions at 5.02 TeV, and for pp collisions at 2.76 and 7 TeV are measured. Using the 2.76 and 7 TeV data, an interpolation by QCD factorization is used to construct a pp reference fragmentation function at 5.02 TeV. This is compared to the measured pPb fragmentation and is found to be consistent within the current statistical and systematic uncertainty.

References

[1] CMS Collaboration, "Nuclear effects on the transverse momentum spectra of charged particles in pPb collisions at $\sqrt{s_{NN}} = 5.02$ TeV", *Eur. Phys. J.* **C75** (2015), no. 5, 237, doi:10.1140/epjc/s10052-015-3435-4, arXiv:1502.05387.

[2] ATLAS Collaboration, "Charged hadron production in p+Pb collisions at $\sqrt{s_{NN}} = 5.02$ TeV measured at high transverse momentum by the ATLAS experiment",.

[3] M. L. Miller, K. Reygers, S. J. Sanders, and P. Steinberg, "Glauber modeling in high energy nuclear collisions", *Ann. Rev. Nucl. Part. Sci.* **57** (2007) 205–243, doi:10.1146/annurev.nucl.57.090506.123020, arXiv:nucl-ex/0701025.

[4] H. Paukkunen, "The LHC p+Pb run from the nuclear PDF perspective", *PoS* **DIS2014** (2014) 053, arXiv:1408.4657.

[5] ATLAS Collaboration, "Centrality and rapidity dependence of inclusive jet production in $\sqrt{s_{\mathrm{NN}}}$ = 5.02 TeV proton–lead collisions with the ATLAS detector", arXiv:1412.4092.

[6] CMS Collaboration, "Measurement of inclusive jet nuclear modification factor in pPb collisions at $\sqrt{s_{\mathrm{NN}}} = 5.02$ TeV with CMS", CMS Physics Analysis Summary CMS-PAS-HIN-14-001, CERN, 2014.

[7] M. Cacciari, G. P. Salam, and G. Soyez, "The anti-k_t jet clustering algorithm", *JHEP* **04** (2008) 063, doi:10.1088/1126-6708/2008/04/063, arXiv:0802.1189.

[8] CMS Collaboration, "Particle-Flow Event Reconstruction in CMS and Performance for Jets, Taus, and MET", CMS Physics Analysis Summary CMS-PAS-PFT-09-001, CERN, 2009.

[9] CMS Collaboration, "Commissioning of the Particle-Flow reconstruction in Minimum-Bias and Jet Events from pp Collisions at 7 TeV", CMS Physics Analysis Summary CMS-PAS-PFT-10-002, CERN, 2010.

[10] CMS Collaboration, "Tracking and Vertexing Results from First Collisions", CMS Physics Analysis Summary CMS-PAS-TRK-10-001, CERN, 2010.

[11] T. Sjöstrand, S. Mrenna, and P. Skands, "PYTHIA 6.4 Physics and Manual", *JHEP* **05** (2006) 026, arXiv:hep-ph/0603175.

[12] X.-N. Wang and M. Gyulassy, "HIJING: A Monte Carlo model for multiple jet production in pp, pA and AA collisions", *Phys. Rev. D* **44** (1991) 3501–3516, doi:10.1103/PhysRevD.44.3501.

[13] M. Gyulassy and X.-N. Wang, "HIJING 1.0: A Monte Carlo program for parton and particle production in high-energy hadronic and nuclear collisions", *Comput. Phys. Commun.* **83** (1994) 307, doi:10.1016/0010-4655(94)90057-4, arXiv:nucl-th/9502021.

[14] M. Cacciari, G. P. Salam, and G. Soyez, "FastJet User Manual", *Eur. Phys. J.* **C72** (2012) 1896, doi:10.1140/epjc/s10052-012-1896-2, arXiv:1111.6097.

[15] CMS Collaboration, "Studies of dijet transverse momentum balance and pseudorapidity distributions in pPb collisions at $\sqrt{s_{\mathrm{NN}}} = 5.02$ TeV", *Eur. Phys. J.* **C74** (2014), no. 7, 2951, doi:10.1140/epjc/s10052-014-2951-y, arXiv:1401.4433.

[16] R. Field, "Early LHC Underlying Event Data — Findings and Surprises", in *HCP 2010, Proc. 22nd Hadron Collider Physics Conference*, W. Trischuk, ed. Toronto, Canada, 2010. arXiv:1010.3558.

[17] CMS Collaboration, "Determination of Jet Energy Calibration and Transverse Momentum Resolution in CMS", *JINST* **6** (2011) P11002, doi:10.1088/1748-0221/6/11/P11002, arXiv:1107.4277.

[18] NNPDF Collaboration, "Unbiased global determination of parton distributions and their uncertainties at NNLO and at LO", *Nucl. Phys. B* **855** (2012) 153–221, doi:10.1016/j.nuclphysb.2011.09.024, arXiv:1107.2652.

[19] CDF Collaboration, "Erratum: Measurement of particle production and inclusive differential cross sections in $p\bar{p}$ collisions at $\sqrt{s}$ = 1.96 TeV [Phys. Rev. D79 (2009) 112005]", *Phys. Rev.* **D82** (2010) 119903, doi:doi:10.1103/PhysRevD.82.119903.

[20] CMS Collaboration, "Charged particle transverse momentum spectra in pp collisions at $\sqrt{s}$ = 0.9 and 7 TeV", *JHEP* **08** (2011) 086, doi:10.1007/JHEP08(2011)086, arXiv:1104.3547.

[21] CMS Collaboration, "Study of high-p_T charged particle suppression in PbPb compared to pp collisions at $\sqrt{s_{\mathrm{NN}}}$ = 2.76 TeV", *Eur. Phys. J.* **72** (2012) 1945, doi:10.1140/epjc/s10052-012-1945-x, arXiv:1202.2554.